

On the energy spectrum of rapidly rotating forced turbulence

Manohar K. Sharma,^{1, a)} Mahendra K. Verma,^{1, b)} and Sagar Chakraborty^{1, c)}

Department of Physics, Indian Institute of Technology Kanpur, Uttar Pradesh 208016, India

In this paper, we investigate the statistical features of the fully developed, forced, rapidly rotating, turbulent system using numerical simulations, and model the energy spectrum that fits well with the numerical data. Among the wavenumbers (k) larger than the Kolmogorov dissipation wavenumber, the energy is distributed such that the suitably non-dimensionalized energy spectrum is $\bar{E}(\bar{k}) \approx \exp(-0.05\bar{k})$, where overbar denotes appropriate non-dimensionalization. For the wavenumbers smaller than that of forcing, the energy in a horizontal plane is much more than that along the vertical rotation-axis. For such wavenumbers, we find that the anisotropic energy spectrum, $E(k_{\perp}, k_{\parallel})$ follows the power law scaling, $k_{\perp}^{-5/2} k_{\parallel}^{-1/2}$, where ‘ \perp ’ and ‘ \parallel ’ respectively refer to the directions perpendicular and parallel to the rotation axis; this result is in line with the Kuznetsov–Zakharov–Kolmogorov spectrum predicted by the weak inertial-wave turbulence theory for the rotating fluids.

PACS numbers: 47.27.Jv, 47.32.-Ef, 47.27.ek

I. INTRODUCTION

Rotating turbulence¹—turbulence in rotating fluids—is a commonly occurring phenomenon in the geophysical and the astrophysical flows. It also occurs in the engineering flows like the ones in turbo-machinery and reciprocating engines with swirl and tumble. The large-scale structures of the turbulent system are affected by rotation due to the Coriolis force that acts in the plane perpendicular to the direction of angular velocity. Intriguingly, the scaling law of the energy spectrum in the inertial range changes with the rotation rate in a way so as to two-dimensionalize the three-dimensional (3D) fluid turbulence. It is well known that, Kolmogorov^{2,3} proposed an inertial range energy spectrum for homogeneous and isotropic 3D hydrodynamics turbulence: $E(k) \sim \epsilon^{2/3} k^{-5/3}$, where ϵ is the constant energy dissipation rate. The Kolmogorov spectrum is quite universal and observed in plethora of other realistic settings, e.g., shear flows⁴, viscoelastic fluids⁵, buoyancy-driven systems^{6,7}, and jet flows⁸. On the other hand, the energy cascade for the two-dimensional (2D) turbulence system shows dual behaviour^{9–13}: an inverse cascade at large scales with $E(k) \sim k^{-5/3}$ and a forward cascade of enstrophy at relatively small scales with $E(k) \sim k^{-3}$.

The energy spectrum becomes more complex in the presence of rotation in the turbulent system and there is no unanimity about the form of the inertial range energy spectrum among the researchers. The largest wavenumber upto which the Coriolis force dominates over the nonlinearity is specified by the Zeman wavenumber, $k_{\Omega} \equiv (\Omega^3/\epsilon)^{1/2}$; larger scales corresponding to $k \lesssim k_{\Omega}$ are affected the most by the rotational effects. Here, Ω is the magnitude of the angular velocity. Be it analytical, numerical, or experimental investigations of either the forced or the decaying rotating turbulent fluid, it is generally found^{14–39} that the energy spectrum for the rotation dominated wavenumbers scales as k^{-m} where $m \in [2, 3]$. Apart from these power-law scalings for relatively larger scales, the energy spectrum for the smaller scales in rotating turbulence is equally enigmatic. In addition to the characteristic

^{a)}Electronic mail: kmanohar@iitk.ac.in

^{b)}Electronic mail: mkv@iitk.ac.in

^{c)}Electronic mail: sagarc@iitk.ac.in

energy spectrum, the inverse cascade of energy is a prominent feature of rotating turbulence which has been studied experimentally as well as numerically^{23,30,35,40–43}. While one observes^{22,44} forward cascade of energy in the vertical planes (the planes containing the direction of rotation), as far as the horizontal planes are concerned, there usually is a forward cascade of energy at the small horizontal scales and an inverse energy cascade at the large horizontal scales. The inverse cascade yields coherent columnar structures in the flow. There are also evidences^{35,45} of non local energy transfers in rotating turbulence.

In nonrotating 3D turbulent fluids, subsequent to a model proposed by Kraichnan⁴⁶ for the kinetic energy spectrum in far dissipation range, Pao⁴⁷ and Pope⁴⁸ separately proposed models which are applicable in both the inertial as well as the dissipation ranges. These two model spectra respectively are $E(k) = K_o \epsilon^{2/3} k^{-5/3} \exp(-\frac{3}{2} \alpha \nu \epsilon^{-1/3} k^{4/3})$, where K_o is Kolmogorov constant and ν is the kinematic viscosity; and $E(k) = C \epsilon^{2/3} k^{-5/3} f_L(kL) f_\eta(k\eta)$, where C is a real constant, L is the integral length scale, η is the Kolmogorov length scale, and f_L and f_η are two non-dimensional functions⁴⁸. Another widely used typical phenomenological form of the energy spectrum in far dissipation range of 3D isotropic homogeneous turbulence is given by $E(k) \sim (k/k_\eta)^\gamma \exp[-\beta(k/k_\eta)^n]$, where γ , β , and n are real constants and k_η is the Kolmogorov dissipation scale. The values of γ , β and n are often debated in turbulence community. While $n = 1$ (cf. Smith and Reynolds⁴⁹ supporting $n = 2$) is agreed upon by many researchers^{50–54}, there is relatively more disagreement about the value^{46,55–57} of γ ($= 3, -1.6, -2, 3.3$) and the value^{55,57,58} of β ($= 4.9, 7.1, 5.2$). Needless to say, as far as the more complex problem of the forced rotating turbulence is concerned, the issue of such an energy spectrum is even wider open. Given the uncertainty in the two exponents, the usage of this energy spectrum is debatable. In fact, to the best of our knowledge, no one has reported such an energy spectrum for smaller scales that extend far into the dissipation range of the forced rotating fluid turbulence.

Recently, Sharma et al.⁵⁹ have investigated the statistical behaviour of the rapidly rotating decaying turbulence. They have reported that a major fraction of the total energy is confined in the Fourier modes $(\pm 1, 0, 0)$ and $(0, \pm 1, 0)$, which correspond to the largest coherent columnar structure in the flow. These modes contains approximately 85 percent of total energy of the system. Further, they have also proposed a model for the energy spectrum: $E(k) \sim C \epsilon_\omega^{2/3} k^{-3} \exp[-C(k/k_d)^2]$ in the region $k \geq 2k_\eta$. Here $k_d \equiv \epsilon^{1/6}/\sqrt{\nu}$, ϵ_ω is the enstrophy dissipation rate, C is a constant, and k_η is the Kolmogorov dissipation wavenumber. There is no reason to believe *a priori* that these results should hold good for the forced rotating turbulence system. In fact, the introduction of forcing at an intermediate scale—corresponding wavenumber being k_f —breaks the kinetic energy spectrum into two disjoint region: larger scales $k < k_f$ and smaller scales $k > k_f$. Contrary to what has been observed in the decaying case, the energy spectrum in the forced case shows power law scaling close to $E(k_\perp, k_\parallel) \sim k_\perp^{-5/2} k_\parallel^{-1/2}$ in highly anisotropic large scales. (The subscripts ‘ \perp ’ and ‘ \parallel ’ respectively refer to the directions perpendicular and parallel to the rotation axis.) In the rather isotropic far dissipation range, the energy spectrum becomes exponential function of ‘ $-k$ ’. Additionally, although we have observed that $(\pm 1, 0, 0)$ and $(0, \pm 1, 0)$ still contain a major fraction of the total energy, the energy content in the intermediate and the smaller scales is much more than that for the decaying rotating turbulent; as a result, one observes rather diffused columnar structures in case of forced rotating turbulence. The main aim of our paper is to elaborate on these interesting results and to contrast the forced turbulence with the decaying one.

However, before we start presenting the results in a systematic manner, let us clearly describe our model system.

II. THE MODEL SYSTEM

The governing equation of a forced incompressible fluid flow in the rotating reference frame is:

$$\frac{\partial \mathbf{u}}{\partial t} + (\mathbf{u} \cdot \nabla) \mathbf{u} = -\nabla p - 2\boldsymbol{\Omega} \times \mathbf{u} + \nu \nabla^2 \mathbf{u} + \mathbf{f}, \quad (1)$$

$$\nabla \cdot \mathbf{u} = 0, \quad (2)$$

where \mathbf{u} is the velocity field, $\boldsymbol{\Omega} = \Omega \hat{z}$ is the angular velocity of the rotating frame, p is the pressure field which includes contributions from centrifugal acceleration, ν is the kinematic viscosity, $-2\boldsymbol{\Omega} \times \mathbf{u}$ is the Coriolis acceleration, and \mathbf{f} is the force field.

We have simulated these equations in a cube of size $(2\pi)^3$ with periodic boundary condition on all the sides using pseudo-spectral code, Tarang^{60,61}. We have used fourth-order Runge-Kutta method for time stepping, and Courant-Friedrich-Lewy (CFL) condition to optimize the time stepping (Δt) and 2/3 rule for dealiasing. Our simulations are with grid-resolutions of 512^3 and 1024^3 , and a constant rotation rate $\Omega = 32$ which corresponds to Rossby number (Ro) of the order of 10^{-3} . One may recall that $\text{Ro} \equiv U/\Omega L$, where U and L respectively being the large scale velocity and the corresponding length scale, is the ratio of the magnitudes of $(\mathbf{u} \cdot \nabla) \mathbf{u}$ and the Coriolis acceleration. We have used our forcing scheme in such a way that it supplies constant energy and no kinetic helicity in the flow. In the Fourier space the forcing function ($\hat{\mathbf{f}}(\mathbf{k})$) is taken as,

$$\hat{\mathbf{f}}(\mathbf{k}) = \frac{\epsilon_{in} \hat{\mathbf{u}}(\mathbf{k})}{n_f [\hat{\mathbf{u}}(\mathbf{k}) \hat{\mathbf{u}}^*(\mathbf{k})]}, \quad (3)$$

where n_f is the total number of modes at which the forcing is active, and ϵ_{in} is the energy input rate. The phase of $\hat{\mathbf{f}}(\mathbf{k})$ is chosen randomly at every time step. Other relevant parameters of our simulations are tabulated in Table I.

TABLE I. Parameters of the simulation: the grid-resolution N , the forcing wavenumber band k_f , rotation rate Ω , kinematic viscosity ν , final eddy turn-over time t_f , energy supply rate ϵ , Rossby number Ro, Reynolds number Re, Zeman wavenumber k_Ω , $k_{\max}\eta$, and the Kolmogorov dissipation wavenumber k_η .

N	512^3	1024^3
k_f	40 – 41	80 – 82
Ω	32	32
ν	0.001	0.001
t_f	56	3
ϵ	0.40	0.80
Ro	0.007	0.005
Re	1736	1786
k_Ω	286	202
k_η	141	168
$k_{\max}\eta$	4.4	3.0

We have used the data corresponding to the time frame $t = 45$ of 512^3 grid resolution as an initial condition for 1024^3 grid. The system evolve up to $t = 3$ eddy turn-over time for 1024^3 grid. We find that $k_{\max}\eta > 1.5$ for the simulation, where η is the Kolmogorov's length scale, which shows our simulation is well resolved. We have also ensured that the data is collected from the steady state. Additionally, by working with the two grid-resolutions, the results presented in this paper have been shown to be grid independent.

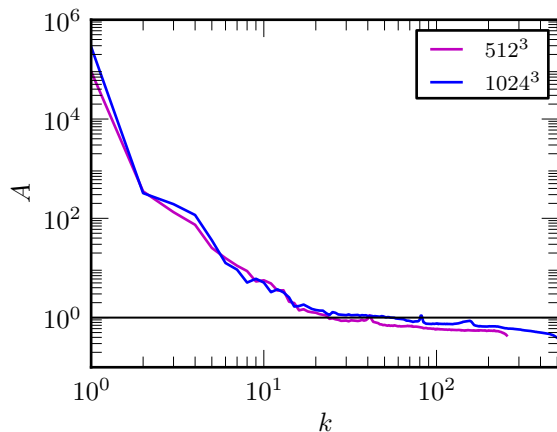


FIG. 1. Anisotropy of the forced rotating turbulent system vs. wavenumber at $t = t_f$ for grid simulation of 512^3 grid resolution (magenta) and 1024^3 grid resolution (blue).

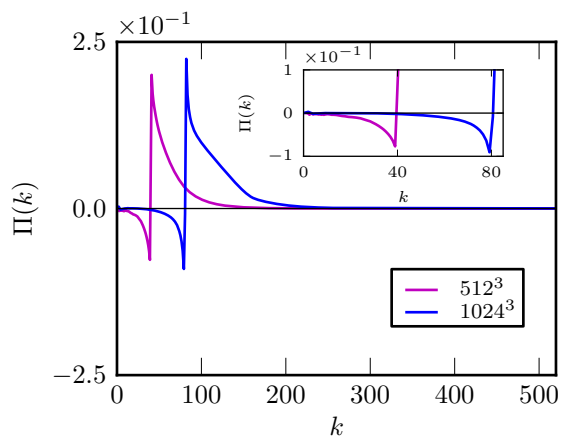


FIG. 2. Plot of kinetic energy flux $\Pi(k)$ vs. k of the 3D velocity field at $t = t_f$ for grid resolution 512^3 (magenta) and 1024^3 grid resolution (blue). The peaks in the plots indicate the corresponding forced wavenumbers k_f .

III. QUASI-TWO-DIMENSIONALIZATION

Coriolis force affects the perpendicular components of velocity field $\mathbf{u}_\perp = u_x \hat{\mathbf{x}} + u_y \hat{\mathbf{y}}$, and this force is the primary reason for the quasi-two-dimensionalization (2D) of three-dimensional (3D) turbulent flow. Below we present evidences for the quasi-two-dimensional nature of the flow.

A. Strong anisotropy

We know that, by definition, the Coriolis force is dominant at wavenumbers smaller than the Zeman wavenumber. In Fig. 1 we plot the anisotropy parameter $A \equiv E_\perp/2E_\parallel$ as a

function of wavenumber. Here, $E_{\perp} \equiv E_x + E_y$, and $E_{\parallel} \equiv E_z$ [with $E_x \equiv \int (u_x^2/2) d\mathbf{r}$, $E_y \equiv \int (u_y^2/2) d\mathbf{r}$, and $E_z \equiv \int (u_z^2/2) d\mathbf{r}$]. It is obvious from the figure that there is strong anisotropy ($A \gg 1$), and hence quasi-two-dimensionalization, at larger scales; the energy (E_{\parallel}) in the parallel (to $\boldsymbol{\Omega}$) component of velocity is much less than the average energy (E_{\perp}) in one of the perpendicular components. It is of importance to note that at smaller scales, the system is effectively isotropic since $A \sim 1$, and consequently the flow can be seen as a 3D turbulent flow where the effect of rotation is negligible.

B. Inverse energy cascade

The energy evolution equation may be written as,

$$\frac{\partial E(k, t)}{\partial t} = T(k, t) - 2\nu k^2 E(k, t) + F(k, t), \quad (4)$$

where $T(k, t)$ is the energy transfer to the wavenumber shell k due to nonlinearity, $-2\nu k^2 E(k, t)$ is the energy dissipation spectrum, and $F(k, t)$ is the energy injected in the system by forcing. Away from the forcing scales, in steady state where $\frac{\partial E(k, t)}{\partial t} \approx 0$, Eq. (4) becomes,

$$\frac{d\Pi(k)}{dk} \equiv -T(k) = -2\nu k^2 E(k). \quad (5)$$

$\Pi(k)$ is the kinetic energy flux, defined as the net transfer of energy out of the sphere of radius k by the modes inside the sphere. We can compute the energy flux of the system using the following formula^{62,63}:

$$\Pi(k_*) = \sum_{k > k_*} \sum_{p \leq k_*} S(\mathbf{k}|\mathbf{p}|\mathbf{q}), \quad (6)$$

where

$$S(\mathbf{k}|\mathbf{p}|\mathbf{q}) \equiv \text{Im}[(\mathbf{k} \cdot \mathbf{u}(\mathbf{q}))(\mathbf{u}(\mathbf{p}) \cdot \mathbf{u}^*(\mathbf{k}))], \quad (7)$$

is the mode-to-mode energy transfer rate from the mode \mathbf{p} to mode \mathbf{k} with mode \mathbf{q} as a mediator in a triad $(\mathbf{k}, \mathbf{p}, \mathbf{q}; \mathbf{k} = \mathbf{p} + \mathbf{q})$. The resulting figure, Fig. 2, explicitly depicts that at the scales larger than the scale at which forcing is active, there is inverse cascade of energy that is reminiscent of similar inverse cascade in the two-dimensional turbulence. As a result of this inverse cascade of the kinetic energy, there would be condensation of kinetic energy at lower wavenumber. This is also seen in the decaying rotating turbulent system⁵⁹. This condensation is naturally expected to give rise to the large scale coherent structures.

C. Large scale coherent structures

There is a large body of works^{23,30,59,64–69} on the formation of the large scale structures, which is known to depend on the strength of rotation rate: at a very high rotation rate, the flow profile becomes quasi-two-dimensionalized with sharp coherent vortical columns, while at a low rotation rate, the columnar vortices are understandably disorganized. Figure 3(a) exhibits isosurfaces of constant $|\boldsymbol{\omega}|$ at $t = t_f$, where $\boldsymbol{\omega} = \nabla \times \mathbf{u}$ is the vorticity field. In Fig. 3(b) we plot the 2D velocity ($\mathbf{u} = u_x \hat{\mathbf{x}} + u_y \hat{\mathbf{y}}$) field for the horizontal cross-section taken at $z = \pi$ of the flow profile. The figure shows vortical columns. We observe that the columnar vortices are disorganized and not very sharp in appearance. Compared to the decaying case⁵⁹, in 3D forced rotating turbulence flow, the velocity in the direction of rotation is no longer constant, and the stretching and tilting of vortices occurs. Also, in the plane perpendicular to the direction of rotation, incompressible condition ($\nabla \cdot \mathbf{u}_{\perp} \neq 0$) is not satisfied and the two-dimensionalization is a relatively hindered than what happens in

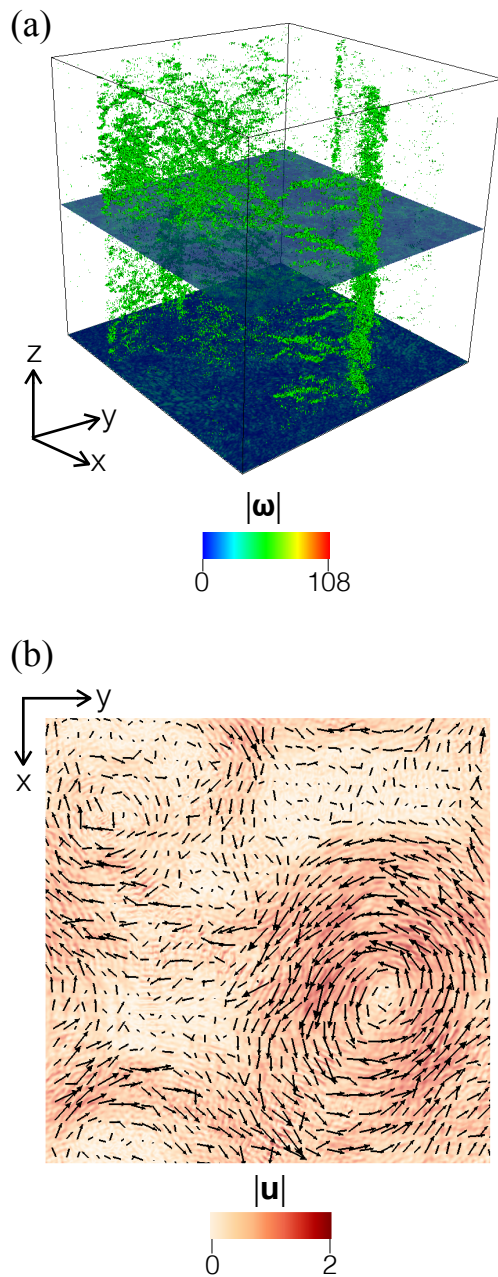


FIG. 3. Plots for (a) iso-surfaces of various magnitudes of the 3D vorticity field, and (b) the density plot for the cross-section of 2D velocity field taken at $z = \pi$. Both the plots use the 1024^3 -grid simulations data.

the decaying case. Additionally, the forcing randomizes the flow, and it starts affecting the velocity field and obstructs the alignment of vorticity field along the direction of rotation. This obstruction in alignment of velocity fields affects the structure formation in the forced rotating turbulent system.

In order to quantitatively understand the disorganization of the columnar structures in forced rotating turbulence, we study the energy content of the Fourier modes. Table II tabulates the energy contents of the most energetic Fourier modes for the forced rotating

case at time frame $t = 56$ for the grid resolution of 512^3 and at $t = 3$ for 1024^3 grid. We do not list the energy of $-\mathbf{k}$ modes because $\mathbf{u}(-\mathbf{k}) = \mathbf{u}^*(\mathbf{k})$. The fraction of total energy contained in $18 \times 2 = 36$ Fourier modes is a significant amount of the total energy spread over 512^3 and 1024^3 modes. The Fourier modes $(k_x, k_y, k_z) = (1, 0, 0)$ and $(0, 1, 0)$ are the most dominant modes of the system. These modes contain 25 to 30 percent of total energy of the system. The situation is different in case of decaying rotating turbulence, where modes $(\pm 1, 0, 0)$ and $(0, \pm 1, 0)$ contain around 90 percent of total energy⁵⁹. It may be remarked that in case of decaying turbulence these modes are not strong initially but later in time they become dominant. In comparison, however, there is no significant temporal variation in the kinetic energy distribution for the forced rotating turbulence, as can be gathered from Table II. The important thing to note is that, in case of the forced rotating turbulent system, more energy is uniformly distributed in the other modes as should be expected for the relatively less coherent columns.

TABLE II. Percentage energy distribution among dominant modes at $t = 56$ and $t = 3$ for the grid resolution of 512^3 and 1024^3 at the rotation rate $\Omega = 32$ respectively. In table E_{mode} is defined as $E_{\text{mode}} = |u(\mathbf{k})|^2/2$, and E is the total energy of the system at $t = 3, 56$.

Mode (k_x, k_y, k_z)	E_{mode}/E (%)	
	$t = 56$ $N = 512^3$	$t = 3.0$ $N = 1024^3$
(1, 0, 0)	14.17	15.02
(0, 1, 0)	11.31	13.97
(1, 1, 0)	1.62	2.82
(-1, 1, 0)	1.43	0.45
(1, 2, 0)	0.92	1.77
(2, -1, 0)	0.51	0.40
(-2, 1, 0)	0.51	0.40
(2, 2, 0)	0.34	0.04
(1, -2, 0)	0.31	0.19
(-3, 1, 0)	0.31	0.22
(2, -2, 0)	0.21	0.12
(3, 1, 0)	0.13	0.06
(3, -2, 0)	0.13	0.06
(2, 1, 0)	0.13	0.23
(-1, -3, 0)	0.07	0.15
(-3, -2, 0)	0.05	0.44
(-2, -3, 0)	0.02	0.13
(-3, 0, 0)	0.02	0.06
Total %:	32.19	36.53

IV. THE ENERGY SPECTRUM

The energy spectrum across the full range of wavenumbers is shown in Fig. 4(a) and Fig. 5. We note that about the forced scales (corresponding to the peaks in the plots), the spectrum is too disrupted to show any prominent scaling. We, thus, focus our attention on two different non-overlapping ranges of scales: the scales smaller than the forcing scales and the scales larger than the forcing scales.

It is obvious that the larger scales, being more affected by the rotation, should behave as if they are quasi-two-dimensionalized. In contrast, the smaller scales should have energy

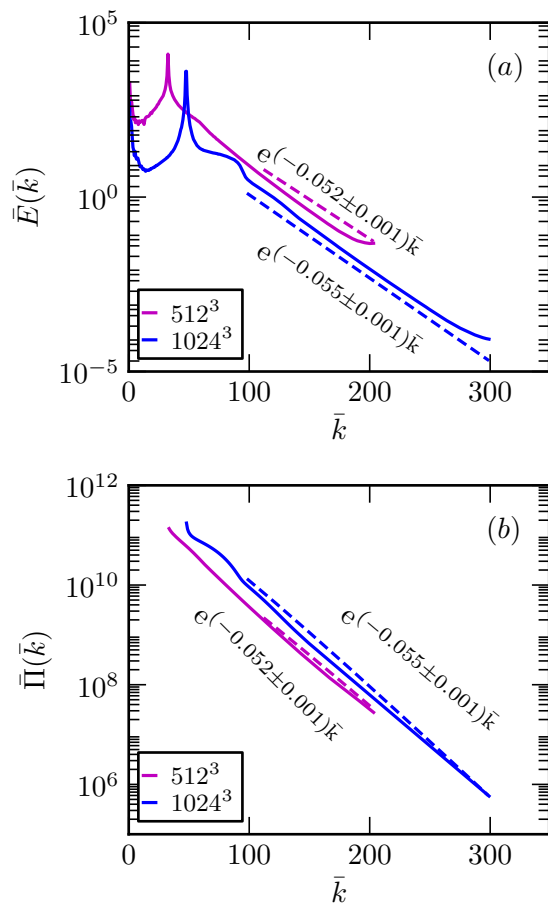


FIG. 4. Plots of (a) the non-dimensionalized energy spectra, $\bar{E}(\bar{k})$, and (b) the non-dimensionalized energy flux, $\bar{\Pi}(\bar{k})$ at $t = t_f$, as generated by the simulations done with grid resolutions of 512^3 (magenta) and 1024^3 (blue) for the forced rotating turbulent fluid. The dotted lines are the fits generated in accordance with the energy spectra and the energy flux given in Eqs. (11)-(12).

spectrum with an exponential term reminding one of the far dissipation range of the 3D isotropic homogeneous turbulence and the exponential fit found for the rapidly rotating decaying turbulence⁵⁹. However, the energy spectra that we report in this paper for both the ranges ($k < k_f$ and $k > k_f$) are—to the best of our knowledge—unreported in any direct numerical simulations done so far. In particular, we find that while the exponential fit in the decaying case goes as $\exp(-\text{constant} \times k^2)$, in the forced case it goes as $\exp(-\text{constant} \times k^1)$ that is less steep in the dissipation range ($k > k_\eta, k_f$). Furthermore, in the anisotropic regime, i.e., in the larger scales ($k < k_f$), the Kuznetsov–Zakharov–Kolmogorov (KZK) spectrum²⁵ emerges. In what follows, we model and discuss these spectra in detail as discovered in our numerical simulations.

A. Model spectrum for smaller scales

Most models of the forced rotating turbulence predict Kolmogorov’s $k^{-5/3}$ spectrum in the wavenumber range: $k_\Omega, k_f < k < k_{\text{DI}}$, where k_{DI} is the transition wavenumber (usually

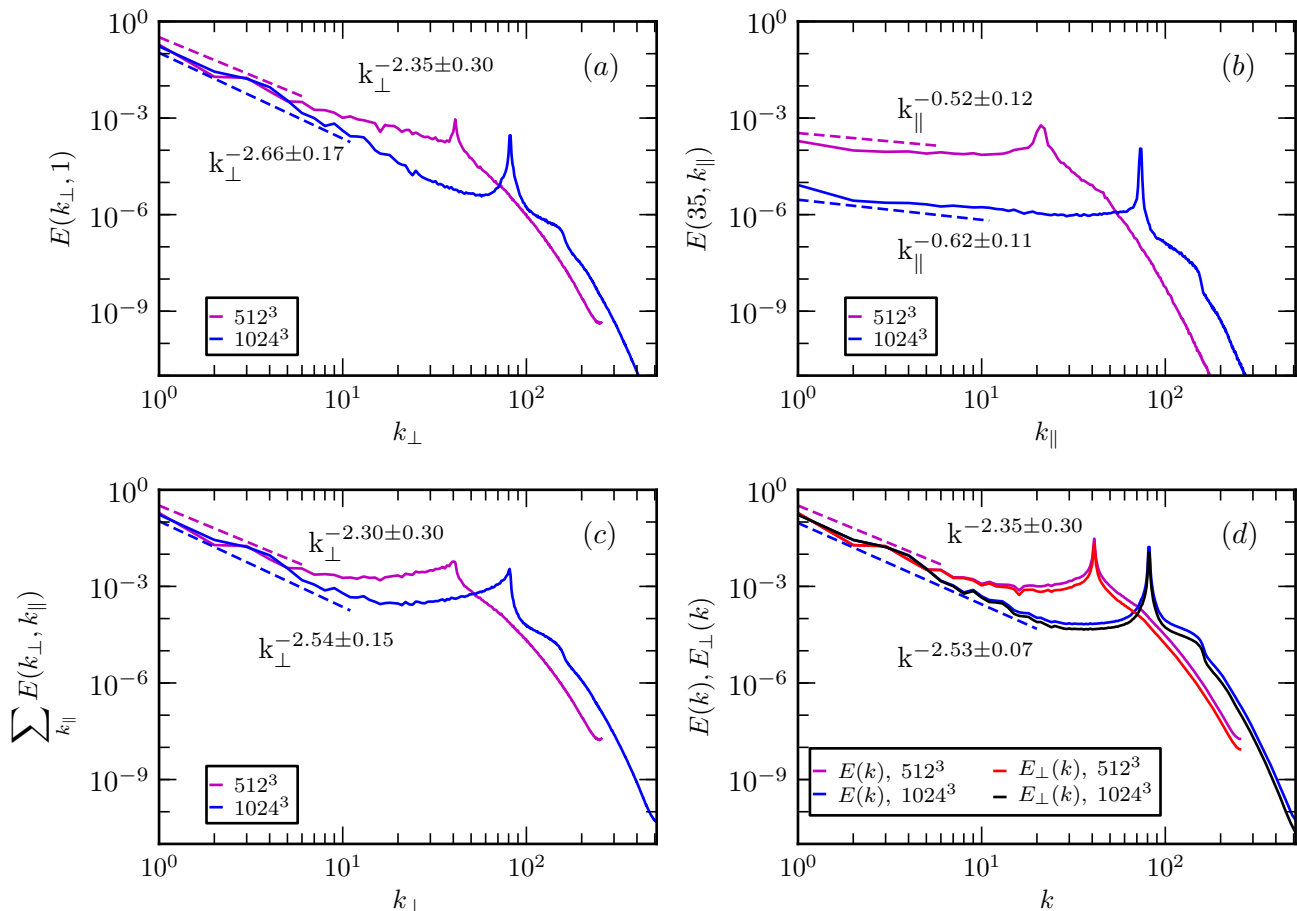


FIG. 5. Plots of the (anisotropic) energy spectrum, $E(k_{\perp}, k_{\parallel})$ at $t = t_f$, as a function of (a) k_{\perp} for $k_{\parallel} = 1$, (b) k_{\parallel} for $k_{\perp} = 35$, and (c) k_{\perp} after the spectrum is summed over all k_{\parallel} . The dashed lines are the fitting lines; we have appropriately used the wavenumber range $1 \leq k_{\perp}, k_{\parallel} \leq 6$ for the 512^3 grid and $1 \leq k_{\perp}, k_{\parallel} \leq 11$ for the 1024^3 grid as the fitting ranges. As in the other plots, we have used magenta for 512^3 grid-resolution data and blue for 1024^3 grid-resolution data. Subplot (d) exhibits the plots for the (isotropic) energy spectra, $E(k)$ (magenta and blue) and $E(k_{\perp})$ (red and black), as functions of k . Here, we have used additional colours—red and black—to respectively indicate the data corresponding to 512^3 grid and 1024^3 grid. The fitting ranges in subplot (d) are $1 \leq k \leq 6$ for 512^3 grid and $1 \leq k \leq 20$ for 1024^3 grid.

much smaller than k_{η}) between the inertial range and the dissipation range. Thus, in order to see this scaling, at the lower end we need to pick the larger one between k_{Ω} and k_f . Unfortunately, in all our simulations, $k_{\Omega} > k_{\eta}$ and k_f is very close to k_{η} that is approximately just two to three times more than k_f . Because of this, there is no significant range of wavenumbers that could exhibit $k^{-5/3}$ spectrum discernible in a log-log plot.

Recently, Verma *et al.*⁷⁰ and Verma⁷ have shown that for laminar hydrodynamic flows, the steady state energy spectrum and the flux are proportional $\exp(-k/k_{\eta})/k$ and $\exp(-k/k_{\eta})$ respectively. These functions satisfy Eq. (5), and also match with numerical simulations of the laminar flows. For our rapidly rotating flow, the energy content in the scales smaller than the forcing scale, $\sum_{k > k_f} E(k)$, is quite small; hence it can be treated as approximately laminar. This is due to the strong inverse cascade of energy to the larger scales that retain

most of the energy. Motivated by this observation, we propose the following form for $E(k)$ in the smaller scales extending into the far dissipation range:

$$E(k) \equiv \sum_{k-1 < k' \leq k} \frac{1}{2} |\hat{\mathbf{u}}(\mathbf{k}')|^2 = u_{\text{rms}}^2 f_L(k) \frac{1}{k} \exp(-\alpha k/k_d). \quad (8)$$

From the form of this $E(k)$, it may be noted that Eq. (5) contains the effects of weak nonlinearity of the flow. The weak energy flux $\Pi(k)$ is the result of this nonlinearity.

The above $E(k)$ has only one exponent, viz., α , that needs to be determined. Here u_{rms} is the rms velocity of the high-pass filtered flow with all the component wave vectors greater than k_η . Note that we have introduced a new wavenumber k_d that is taken to be \sqrt{Re}/L , but now Re is calculated with U replaced by u_{rms} . In this context, recall that $k_\eta \equiv (\epsilon/\nu^3)^{1/4} \sim \sqrt{Re}/L$, where

$$\epsilon = \int_0^\infty 2\nu k^2 E(k) dk = 2\nu u_{\text{rms}}^2 k_d^2 I, \quad (9)$$

with $I \equiv \int_0^\infty \bar{k} f_L(\bar{k}) \exp(-\alpha \bar{k}) d\bar{k}$ and $\bar{k} \equiv k/k_d$. Thus, k_d based on the high-pass filtered flow is analogous to k_η that is based on the unfiltered flow field.

Using \bar{k} , $\bar{E}(\bar{k}) \equiv E(k)k/u_{\text{rms}}^2$, and $\bar{\Pi}(\bar{k}) \equiv \Pi(k)/\epsilon$ as non-dimensionalized quantities, the relationship [Eq. (5)] between the kinetic energy and the energy flux in the non-dimensionalized form becomes:

$$\frac{d\bar{\Pi}(\bar{k})}{d\bar{k}} = -\frac{\bar{k}}{I} \bar{E}(\bar{k}). \quad (10)$$

In the dissipation range $k \gg k_f$, where k_f is the forcing wavenumber and $f_L(\bar{k})$ is unity, the kinetic energy and the energy flux are respectively as follows:

$$\bar{E}(\bar{k}) = \exp(-\alpha \bar{k}), \quad (11)$$

$$\bar{\Pi}(\bar{k}) = \frac{1}{I} \left(\frac{1}{\alpha^2} + \frac{\bar{k}}{\alpha} \right) \exp(-\alpha \bar{k}). \quad (12)$$

It may be easily checked that the above two expressions satisfy the non-dimensionalized equation, Eq. (10).

In Fig. 4(a)-(b), we plot $\bar{E}(\bar{k})$ vs. \bar{k} and $\bar{\Pi}(\bar{k})$ vs. \bar{k} respectively in semi-log scale at time frames $t = 56$ (magenta) for grid resolution of 512^3 and at $t = 3$ (blue) for 1024^3 grid. We observe that the predicted self-consistent model [Eqs. (11)-(12)] of the energy spectrum and the energy flux stands validated by our numerical data in the wavenumber range $k \in [141, 256]$ for 512^3 grid resolution, and $k \in [168, 512]$ for 1024^3 grid resolution. The values of α are 0.052 ± 0.001 for 512^3 grid resolution, and 0.055 ± 0.001 for 1024^3 grid. We are getting approximately same value of α for both the grid resolutions, thus, signifying that the parameter is robust and resolution-independent. The values of Re based on the aforementioned wavenumber ranges are 62 for 512^3 , and 115 for 1024^3 resolutions, which are one order less than the global Re (1736 and 1786 respectively for the grid resolutions 512^3 and 1024^3). Thus, there is reduction in strength of turbulence in the smaller scales, that is the reason why any power law scaling is hard to observe here.

B. Model spectrum near larger scales

Although one can extract scaling exponents from the $E(k)$ vs. k plot to characterise the system, strictly speaking, in the anisotropic regime, the energy spectrum should not be modelled as a function of k . It is more sensible that the energy spectrum be explicitly dependent on both \mathbf{k}_\perp (two dimensional vector perpendicular to the rotation axis) and k_\parallel

(wavenumber corresponding to the direction parallel to the rotation axis). Thus, we define such a spectrum as,

$$E(k_{\perp}, k_{\parallel}) = \sum_{\substack{k_{\perp}-1 < k'_{\perp} \leq k_{\perp}, \\ k_{\parallel}-1 < k'_{\parallel} \leq k_{\parallel}}} \frac{1}{2} |\hat{\mathbf{u}}(k'_{\perp}, k'_{\parallel})|^2. \quad (13)$$

Note that, under the assumption of axisymmetry, we have used the magnitude of \mathbf{k}_{\perp} in the argument of the energy spectrum.

The energy spectrum of the system is calculated by using Eq. (13) and plotted in Fig. 5. In Fig. 5(a)-(b), it is remarkable to note that the energy spectrum observed from our numerical simulation is quite close to the Kuznetsov–Zakharov–Kolmogorov (KZK) spectrum— $E(k) \sim k_{\perp}^{-5/2} k_{\parallel}^{-1/2}$ —within errorbars. The strong rotation supplies a small parameter, Ro , in the framework of weak turbulence. Using this it has shown²⁵ that, in the anisotropic limit $k_{\perp} \gg k_{\parallel}$, structures elongated along the rotation axis are brought forth through dominating local interactions. Further, the KZK spectrum comes out as an exact solution. Although the aforementioned weak turbulence analysis has been done for decaying rotating turbulent fluid, we emphasize that this spectrum appears in our numerical simulations exactly where the system is strongly anisotropic and shows elongated structures, thereby somewhat satisfying the requirements for the appearance of the spectrum. It may be noted, in this context, that the aforementioned plots are for the case: $k_{\perp} \gg k_{\parallel}$, just what the weak turbulence analysis requires. We also note that the shift of the peaks away from k_f in Fig. 5(b) is because the abscissa is k_{\parallel} and not k , and thus, the identity $k^2 = k_{\perp}^2 + k_{\parallel}^2$ with $k = k_f$ and $k_{\perp} = 35$ locates the peaks at $k_{\parallel} \approx 21$ and $k_{\parallel} \approx 74$ respectively for 512^3 and 1024^3 grid resolutions.

Additionally, in Fig. 5(c), we note that the scaling exponent of k_{\perp} is unchanged even when the spectrum is summed over all k_{\parallel} . Further, Fig. 5(d) showcases the fact that this scaling exponent ($\sim -5/2$) is very robust; in the range $A \gg 1$, even the isotropic energy spectrum, $E(k)$, scales as $\sim k^{-5/2}$ and so does $E_{\perp}(k)$ simply because the share of energy contained in the plane perpendicular to the rotation axis is large. We remark, however, the scaling exponent of k_{\parallel} is not very robust and it varies with the choice of k_{\perp} range (see Appendix B). Nevertheless, we believe that ours is the first numerical demonstration of KZK spectra in forced rotating turbulence.

DISCUSSIONS AND CONCLUSION

We have performed direct numerical simulations of a 3D turbulent fluid forced at intermediate scales. The fluid is rotating with a high rotation rate corresponding to $Ro \sim 10^{-3}$. Such a system is known to mimic some of the features of the 2D turbulence. Recall that in the fully developed 2D fluid turbulence—extensively investigated^{10,11,71–79} numerically as well as experimentally—strong vortical structures appear in the system due to inverse cascade of kinetic energy from the forcing scale to the scale corresponding to the box-size. Further, it has been shown that the kinetic energy spectrum for $k < k_f$ is given by $E(k) \sim k^{-5/3}$, whereas^{80–83} for $k > k_f$, $E(k) \sim k^{-3}$.

In the forced rotating flow, we observed that the system becomes highly anisotropic at larger scales; coherent columnar structures are formed but they are relatively more diffused in appearance compared to what is seen in the case of decaying rotating turbulence. We have also found dual cascade regions—forward and reverse cascades—for both the energy and the enstrophy (calculated on a 2D horizontal plane; see Appendix A). While these features are very much reminiscent of the 2D turbulence, the forms of the energy spectrum on the either side of k_f is completely different from what is observed in the 2D turbulence. Thus, the quasi-two-dimensionalization in the rotating 3D turbulent fluid doesn't actually

mean that the spectral properties of the fluid become akin to that possessed by the 2D turbulent fluid.

For the anisotropic regime, we have also investigated the behaviour of the kinetic energy spectrum as a function of k_{\perp} and k_{\parallel} , which is convenient to showcase the manifestations of anisotropic behaviour of system. We observed that the kinetic energy spectrum varies as $k_{\perp}^{-2.35 \pm 0.30}$ in wavenumber range $k_{\perp} \in [1, 6]$ for grid resolution of 512^3 , and scales as $k_{\perp}^{-2.66 \pm 0.30}$ in wavenumber range $k_{\perp} \in [1, 11]$ for grid resolution of 1024^3 . The kinetic energy spectrum as a function of k_{\parallel} shows power scalings for fixed k_{\perp} , specifically, $E(35, k_{\parallel}) \sim k_{\parallel}^{-0.52 \pm 0.12}$ in wavenumber range $k_{\parallel} \in [1, 6]$ for grid resolution of 512^3 and $E(35, k_{\parallel}) \sim k_{\parallel}^{-0.62 \pm 0.11}$ in wavenumber range $k_{\parallel} \in [1, 11]$ for 1024^3 grid. Within the error bars, these scalings are in conformity with the KZK-spectrum. As far as the isotropic small scales are concerned, we have proposed a model [Eq. (8)] that faithfully captures the behaviour of the kinetic energy spectrum in far dissipation range. Our proposed model is in very good agreement with the numerical results over the wavenumber range $k \in [k_{\eta}, k_{\max}]$.

Our investigation highlights that the statistical features of the decaying rotating turbulence and the forced rotating turbulence are quite different. This fact suggests that a similar scientific comparison of the decaying versus the forced turbulences under the simultaneous effects of the rotation and the non-zero kinetic helicity is worth pursuing in future. This is important because, in any realistic experiment of the forced rotating turbulence, the experimental set-ups are such that some finite amount of the kinetic helicity would invariably be imparted to the fluid. Also, the kinetic helicity is significant inside the Earth's outer core, and is similarly important in the other planets and the stars.

ACKNOWLEDGEMENTS

The authors thank Abhishek Kumar for many important suggestions. MKV thanks the Department of Science and Technology, India (INT/RUS/RSF/P-03) and Russian Science Foundation Russia (RSF-16-41-02012) for the Indo-Russian project. SC gratefully acknowledges financial support from the INSPIRE faculty fellowship (DST/INSPIRE/04/2013/000365) awarded by the INSA, India and DST, India. The simulations were performed on the HPC2010 and HPC2013 and Chaos cluster of IIT Kanpur, India.

Appendix A: Inverse Enstrophy Cascade

We studied the enstrophy flux of plane perpendicular to the axis of rotation. We compute the enstrophy flux of the 2D velocity field \mathbf{u}_{\perp} at the plane using the formula:

$$\Pi_{\omega}^{(2D)}(k_*) = \sum_{k > k_*} \sum_{p \leq k_*} S^{\omega\omega}(\mathbf{k}|\mathbf{p}|\mathbf{q}). \quad (\text{A1})$$

Here,

$$S^{\omega\omega}(\mathbf{k}|\mathbf{p}|\mathbf{q}) = \text{Im} [(\mathbf{k} \cdot \mathbf{u}_{\perp}(\mathbf{q})) (\omega_z(\mathbf{p})\omega_z^*(\mathbf{k}))], \quad (\text{A2})$$

with,

$$\omega_z(\mathbf{k}) = [i\mathbf{k} \times \mathbf{u}(\mathbf{k})]_z, \quad (\text{A3})$$

represents the enstrophy transfer from mode $\omega_z(\mathbf{p})$ to mode $\omega_z(\mathbf{k})$ with mode $\mathbf{u}(\mathbf{q})$ acting as a mediator. Figure 6 illustrate the enstrophy flux of the horizontal cross-section taken at $z = \pi$ at time frame $t = 56$ (magenta) for grid resolution of 512^3 and at $t = 3$ (blue) for 1024^3 grid. Arguably⁸³, when the vortex merger is strong in 2D turbulent flow, the mean enstrophy flux is negative^{84,85} for the scales larger than the injection scales. Therefore, the negative enstrophy flux in the scales larger than the injection scale (as exhibited in Fig. 6) signifies that our rotating 3D flow is appreciably two-dimensionalized.

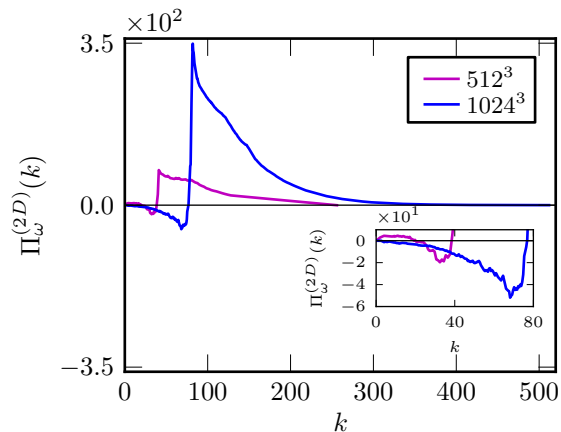


FIG. 6. Plot of the 2D enstrophy flux, $\Pi_{\omega}^{(2D)}(k)$, for the 2D velocity field on the horizontal cross-section, $z = \pi$, at $t = t_f$ for the grid-resolutions 512^3 (magenta) and 1024^3 (blue). The inset highlights the inverse cascade of the flux. The peaks in the plots indicate the corresponding forced wavenumbers k_f .

Appendix B: Anisotropic Energy Spectrum's Scaling With k_{\parallel}

The KZK spectrum exists in the anisotropic limit, viz., $k_{\perp} \gg k_{\parallel}$, in rapidly rotating turbulence as was shown by Galtier²⁵ (and we have observed so in Fig. 5); however, that analysis did not include forcing. Since our investigation is for the forced rotating turbulent fluid, we must keep this added complication in mind while extracting the exponent of k_{\parallel} in the anisotropic energy spectrum. The scaling of the energy spectrum as a function of k_{\parallel} depends on the choice of k_{\perp} in the anisotropic limit, which is shown in Fig. 7.

In Fig 7, we plot the energy spectrum as a function of k_{\parallel} for different k_{\perp} for both the 512^3 grid resolution and the 1024^3 grid resolution. In order to extract the exponent, we have to not only decide what range of k_{\parallel} to use but also what value of k_{\perp} to choose. Although, one would like to choose a large enough range while maintaining $k_{\perp} \gg k_{\parallel}$, we are restricted in our choice because the peak corresponding to the forcing scale restricts us: the upper bound of the fitting range should ideally be as much away from the forcing scale as possible but the peak shift towards lower wave number, in line with the identity $-k^2 = k_{\perp}^2 + k_{\parallel}^2$, as k_{\perp} increases, thereby making the range smaller. This is at odds with the fact that k_{\perp} must be much greater than k_{\parallel} for witnessing the KZK spectrum. Thus, it effectively becomes a matter of systematic investigation where one should work with all possible combinations of the k_{\parallel} -ranges and the value of k_{\perp} . What we can definitely conclude from Fig. 7 is that for 512^3 grid resolution, the range $1 \leq k_{\parallel} \leq 6$ and $k_{\perp} = 35$ make an ideal combination which leads to the observation of the KZK-spectrum in the anisotropic limit in the forced rotating turbulence. Similar conclusion can be made for the 1024^3 grid resolution with the range $1 \leq k_{\parallel} \leq 11$ and $k_{\perp} = 35$.

¹P. A. Davidson, *Turbulence in Rotating, Stratified and Electrically Conducting Fluids* (Cambridge University Press, Cambridge(UK), 2013).

²A. N. Kolmogorov, "The local structure of turbulence in incompressible viscous fluid for very large Reynolds numbers," *Dokl Acad Nauk SSSR* **30**, 301–305 (1941).

³A. N. Kolmogorov, "Dissipation of Energy in Locally Isotropic Turbulence," *Dokl Acad Nauk SSSR* **32**, 16–18 (1941).

⁴G. E. Elsinga and Ivan Marusic, "The anisotropic structure of turbulence and its energy spectrum," *Phys. Fluids* **28**, 011701 (2016).

⁵P. C. Valente, C. B. da Silva, and F. T. Pinho, "Energy spectra in elasto-inertial turbulence," *Phys. Fluids* **28**, 075108 (2016).

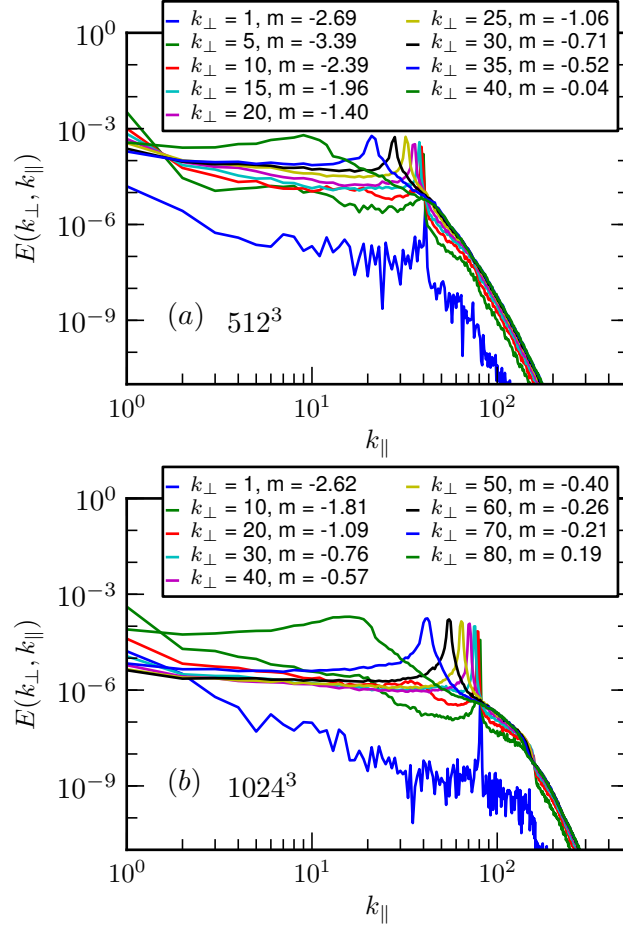


FIG. 7. Plots of the (anisotropic) energy spectrum, $E(k_{\perp}, k_{\parallel})$ at $t = t_f$, as a function of k_{\parallel} with different k_{\perp} for (a) 512^3 grid resolution and (b) 1024^3 grid resolution. The fitting exponent (m) in $E(k_{\perp}, k_{\parallel}) \sim k_{\parallel}^{-m}$ has been calculated in the wavenumber range $1 \leq k_{\parallel} \leq 6$ for the 512^3 grid resolution and $1 \leq k_{\parallel} \leq 11$ for the 1024^3 grid resolution is shown in the legends.

- ⁶S. S. Pawar and J. H. Arakeri, “Kinetic energy and scalar spectra in high rayleigh number axially homogeneous buoyancy driven turbulence,” *Phys. Fluids* **28**, 065103 (2016).
- ⁷M. K. Verma, *Physics of Buoyant Flows, From Instabilities to Turbulence* (World Scientific, Singapore, Singapore, 2018).
- ⁸P. Buchhave and C. M. Velte, “Measurement of turbulent spatial structure and kinetic energy spectrum by exact temporal-to-spatial mapping,” *Phys. Fluids* **29**, 085109 (2017).
- ⁹R. H. Kraichnan, “Inertial ranges in two-dimensional turbulence,” *Phys. Fluids* **10**, 1417 (1967).
- ¹⁰J. Paret and P. Tabeling, “Experimental observation of the two-dimensional inverse energy cascade,” *Phys. Rev. Lett.* **79**, 4162 (1997).
- ¹¹S. Chen, R. E. Ecke, G. L. Eyink, M. Rivera, M. Wan, and Z. Xiao, “Physical mechanism of the two-dimensional inverse energy cascade,” *Phys. Rev. Lett.* **96**, 084502 (2006).
- ¹²A. Vallgren and E. Lindborg, “The enstrophy cascade in forced two-dimensional turbulence,” *J. Fluid Mech.* **671**, 168–183 (2011).
- ¹³G. Boffetta and R. E. Ecke, “Two-Dimensional Turbulence,” *Annu. Rev. Fluid Mech.* **44**, 427–451 (2012).
- ¹⁴A. Ibbetson and D. J. Tritton, “Experiments on turbulence in a rotating fluid,” *J. Fluid Mech.* **68**, 639–672 (1975).
- ¹⁵E. J. Hopfinger, F. K. Browand, and Y. Gagne, “Turbulence and waves in a rotating tank,” *J. Fluid Mech.* **125**, 505–534 (1982).
- ¹⁶J. Bardina, J. H. Ferziger, and R. S. Rogallo, “Effect of rotation on isotropic turbulence - Computation

- and modelling,” *J. Fluid Mech.* **154**, 321–336 (1985).
- ¹⁷L. Jacquin, O. Leuchter, C. Cambon, and J. Mathieu, “Homogeneous turbulence in the presence of rotation,” *J. Fluid Mech.* **220**, 1–52 (1990).
- ¹⁸O. Zeman, “A note on the spectra and decay of rotating homogeneous turbulence,” *Phys. Fluids* **6**, 3221–3224 (1994).
- ¹⁹Y. Zhou, “A phenomenological treatment of rotating turbulence,” *Phys. Fluids* **7**, 2092 (1995).
- ²⁰V. M. Canuto and M. S. Dubovikov, “Physical regimes and dimensional structure of rotating turbulence,” *Phys. Rev. Lett.* **78**, 666–669 (1997).
- ²¹V. M. Canuto and M. S. Dubovikov, “A dynamical model for turbulence. V. The effect of rotation,” *Phys. Fluids* **9**, 2132–2140 (1997).
- ²²P. K. Yeung and Y. Zhou, “Numerical study of rotating turbulence with external forcing,” *Phys. Fluids* **10**, 2895–2909 (1998).
- ²³L. M. Smith and F. Waleffe, “Transfer of energy to two-dimensional large scales in forced, rotating three-dimensional turbulence,” *Phys. Fluids* **11**, 1608 (1999).
- ²⁴C. N. Baroud, B. B. Plapp, Z.-S. She, and H. L. Swinney, “Anomalous self-similarity in a turbulent rapidly rotating fluid,” *Phys. Rev. Lett.* **88**, 114501 (2002).
- ²⁵S. Galtier, “Weak inertial-wave turbulence theory,” *Phys. Rev. E* **68**, 015301–4 (2003).
- ²⁶Y. Hattori, R. Rubinstein, and A. Ishizawa, “Shell model for rotating turbulence,” *Phys. Rev. E* **70**, 046311 (2004).
- ²⁷X. Yang and J. A. Domaradzki, “Large eddy simulations of decaying rotating turbulence,” *Phys. Fluids* **16**, 4088–4104 (2004).
- ²⁸J. E. Ruppert-Felsot, O. Praud, E. Sharon, and H. L. Swinney, “Extraction of coherent structures in a rotating turbulent flow experiment,” *Phys. Rev. E* **72**, 016311 (2005).
- ²⁹L. M. Smith and Y. Lee, “On near resonances and symmetry breaking in forced rotating flows at moderate Rossby number,” *J. Fluid Mech.* **535**, 111–142 (2005).
- ³⁰C. Morize, F. Moisy, and M. Rabaud, “Decaying grid-generated turbulence in a rotating tank,” *Phys. Fluids* **17**, 095105 (2005).
- ³¹W.-C. Müller and M Thiele, “Scaling and energy transfer in rotating turbulence,” *EPL* **77**, 34003 (2007).
- ³²S. Chakraborty and J. K. Bhattacharjee, “Third-order structure function for rotating three-dimensional homogeneous turbulent flow,” *Phys. Rev. E* **76**, 036304 (2007).
- ³³S. Chakraborty, “Signatures of two-dimensionalisation of 3D turbulence in the presence of rotation,” *EPL* **79**, 14002 (2007).
- ³⁴M. Thiele and W.-C. Müller, “Structure and decay of rotating homogeneous turbulence,” *J. Fluid Mech.* **637**, 425–442 (2009).
- ³⁵P. D. Mininni, A. Alexakis, and A. Pouquet, “Scale interactions and scaling laws in rotating flows at moderate Rossby numbers and large Reynolds numbers,” *Phys. Fluids* **21**, 015108 (2009).
- ³⁶S. Chakraborty, M. H. Jensen, and A. Sarkar, “On two-dimensionalization of three-dimensional turbulence in shell models,” *Eur. Phys. J. B* **73**, 447–453 (2010).
- ³⁷A. Sen, P. D. Mininni, D. Rosenberg, and A. Pouquet, “Anisotropy and nonuniversality in scaling laws of the large-scale energy spectrum in rotating turbulence,” *Phys. Rev. E* **86**, 036319 (2012).
- ³⁸L. Biferale, F. Bonaccorso, I. M. Mazzitelli, M. A. T. van Hinsberg, A. S. Lanotte, S. Musacchio, P. Perlekar, and F. Toschi, “Coherent Structures and Extreme Events in Rotating Multiphase Turbulent Flows,” *Phys. Rev. X* **6**, 041036 (2016).
- ³⁹Y. B. Baqui, P. A. Davidson, and A. Ranjan, “Are there two regimes in strongly rotating turbulence?,” *Phys. Fluids* **28**, 045103 (2016).
- ⁴⁰M. Hossain, “Reduction in the dimensionality of turbulence due to a strong rotation,” *Phys. Fluids* **6**, 1077–1080 (1994).
- ⁴¹L. M. Smith, J. R. Chasnov, and F. Waleffe, “Crossover from two- to three-dimensional turbulence,” *Phys. Rev. Lett.* **77**, 2467–2470 (1996).
- ⁴²A. Pouquet, A. Sen, D. Rosenberg, P. D. Mininni, and J Baerenzung, “Inverse cascades in turbulence and the case of rotating flows,” *Phys. Scr.* **T155**, 014032 (2013).
- ⁴³E. Yarom, Y. Vardi, and E. Sharon, “Experimental quantification of inverse energy cascade in deep rotating turbulence,” *Phys. Fluids* **25**, 085105 (2013).
- ⁴⁴A. Campagne, B. Gallet, F. Moisy, and P.-P. Cortet, “Direct and inverse energy cascades in a forced rotating turbulence experiment,” *Phys. Fluids* **26**, 125112 (2014).
- ⁴⁵L. Bourouiba, D. N. Straub, and M. L. Waite, “Non-local energy transfers in rotating turbulence at intermediate Rossby number,” *J. Fluid Mech.* **690**, 129–147 (2011).
- ⁴⁶R. H. Kraichnan, “The structure of isotropic turbulence at very high Reynolds numbers,” *J. Fluid Mech.* **5**, 497–543 (1959).
- ⁴⁷Y.-H. Pao, “Structure of Turbulent Velocity and Scalar Fields at Large Wavenumbers,” *Phys. Fluids* **8**, 1063 (1965).
- ⁴⁸S. B. Pope, *Turbulent Flows* (Cambridge University Press, Cambridge, 2000).
- ⁴⁹L. M. Smith and W. C. Reynolds, “The dissipation-range spectrum and the velocity-derivative skewness in turbulent flows,” *Phys. Fluids A* **3**, 992 (1991).
- ⁵⁰K. R. Sreenivasan, “On the fine-scale intermittency of turbulence,” *J. Fluid Mech.* **151**, 81–103 (1985).
- ⁵¹C. Foias, O. Manley, and L. Sirovich, “Empirical and stokes eignfunctions and far-dissipative turbulent spectrum,” *Phys. Fluids A* **2**, 464 (1990).

- ⁵²T. Sanada, “Comment on the dissipation-range spectrum in turbulent flows,” *Phys. Fluids A* **4**, 1086 (1992).
- ⁵³O. P. Manley, “The dissipation range spectrum,” *Phys. Fluids A* **4**, 1320 (1992).
- ⁵⁴D. O. Martínez, S. Chen, G. D. Doolen, R. H. Kraichnan, L.-P. Wang, and Y. Zhou, “Energy spectrum in the dissipation range of fluid turbulence,” *J. Plasma Phys.* **57**, 195–201 (1997).
- ⁵⁵S. Kida and Y. Murakami, “Kolmogorov similarity in free decaying turbulence,” *Phys. Fluids* **30**, 2030 (1987).
- ⁵⁶J. A. Domaradzki, “Nonlocal triad interactions and the dissipation range of isotropic turbulence,” *Phys. Fluids A* **4**, 2037 (1992).
- ⁵⁷S. Chen, G. D. Doolen, J. R. Herring, R. H. Kraichnan, S. A. Orszag, and Z.-S. She, “Far-dissipation range of turbulence,” *Phys. Rev. Lett.* **70**, 3051 (1993).
- ⁵⁸S. G. Saddoughi and S. V. Veeravalli, “Local isotropy in turbulent boundary layers at high Reynolds number,” *J. Fluid Mech.* **268**, 333–372 (1994).
- ⁵⁹M. K. Sharma, A. Kumar, M. K. Verma, and S. Chakraborty, “Statistical features of rapidly rotating decaying turbulence: Enstrophy and energy spectra and coherent structures,” *Phys. Fluids* **30**, 045103 (2018).
- ⁶⁰M. K. Verma, A. G. Chatterjee, K. S. Reddy, R. K. Yadav, S. Paul, M. Chandra, and R. Samtaney, “Benchmarking and scaling studies of pseudospectral code Tarang for turbulence simulations,” *Pramana - J. Phys.* **81**, 617–629 (2013).
- ⁶¹A. G. Chatterjee, M. K. Verma, A. Kumar, R. Samtaney, B. Hadri, and R. Khurram, “Scaling of a fast fourier transform and a pseudo-spectral fluid solver up to 196608 cores,” *J Parallel Distrib Comput* **113**, 77 – 91 (2018).
- ⁶²G. Dar, M. K. Verma, and V. Eswaran, “Energy transfer in two-dimensional magnetohydrodynamic turbulence: formalism and numerical results,” *Physica D* **157**, 207–225 (2001).
- ⁶³M. K. Verma, “Statistical theory of magnetohydrodynamic turbulence: recent results,” *Phys. Rep.* **401**, 229–380 (2004).
- ⁶⁴P. Bartello, O. Metais, and M. Lesieur, “Coherent structures in rotating three-dimensional turbulence,” *J. Fluid Mech.* **273**, 1–29 (1994).
- ⁶⁵F. S. Godeferd and L. Lollini, “Direct numerical simulations of turbulence with confinement and rotation,” *J. Fluid Mech.* **393**, 257–308 (1999).
- ⁶⁶P. J. Staplehurst, P. A. Davidson, and S. B. Dalziel, “Structure formation in homogeneous freely decaying rotating turbulence,” *J. Fluid Mech.* **598**, 81–105 (2008).
- ⁶⁷F. Moisy, C. Morize, M. Rabaud, and J. Sommeria, “Decay laws, anisotropy and cyclone–anticyclone asymmetry in decaying rotating turbulence,” *J. Fluid Mech.* **666**, 5–35 (2011).
- ⁶⁸B. Gallet, A. Campagne, P. P. Cortet, and F. Moisy, “Scale-dependent cyclone-anticyclone asymmetry in a forced rotating turbulence experiment,” *Phys. Fluids* **26**, 035108 (2014).
- ⁶⁹A. Ranjan and P. A. Davidson, “Evolution of a turbulent cloud under rotation,” *J. Fluid Mech.* **756**, 488–509 (2014).
- ⁷⁰M. K. Verma, A. Kumar, P. Kumar, S. Barman, A. G. Chatterjee, and R. Samtaney, “Energy fluxes and spectra for turbulent and laminar flows,” Accepted in *Fluid Dynamics*(2018).
- ⁷¹V. Borue, “Spectral exponents of enstrophy cascade in stationary two-dimensional homogeneous turbulence,” *Phys. Rev. Lett.* **71**, 3967 (1993).
- ⁷²L.M. Smith and V. Yakhot, “Bose condensation and small-scale structure generation in a random force driven 2D turbulence.” *Phys. Rev. Lett.* **71**, 352–355 (1993).
- ⁷³G. Boffetta, A. Cenedese, S. Espa, and S. Musacchio, “Effects of friction on 2D turbulence: An experimental study of the direct cascade,” *EPL* **71**, 590–596 (2005).
- ⁷⁴M. A. Rutgers, “Forced 2D turbulence: Experimental evidence of simultaneous inverse energy and forward enstrophy cascades,” *Phys. Rev. Lett.* **81**, 2244 (1998).
- ⁷⁵T. Gotoh, “Energy spectrum in the inertial and dissipation ranges of two-dimensional steady turbulence,” *Phys. Rev. E* **57**, 2984–2991 (1998).
- ⁷⁶N. Schorghofer, “Energy spectra of steady two-dimensional turbulent flows,” *Phys. Rev. E* **61**, 6572–6577 (2000).
- ⁷⁷E. Lindborg and K. Alvelius, “The kinetic energy spectrum of the two-dimensional enstrophy turbulence cascade,” *Phys. Fluids* **12**, 945–947 (2000).
- ⁷⁸T. Ishihara and Y. Kaneda, “Energy spectrum in the enstrophy transfer range of two-dimensional forced turbulence,” *Phys. Fluids* **13**, 544–547 (2001).
- ⁷⁹Q. Chen, S. Chen, G. L. Eyink, and K. R. Sreenivasan, “Kolmogorov’s third hypothesis and turbulent sign statistics,” *Phys. Rev. Lett.* **90**, 254501 (2003).
- ⁸⁰V. Borue, “Inverse energy cascade in stationary two-dimensional homogeneous turbulence,” *Phys. Rev. Lett.* **72**, 1475–1478 (1994).
- ⁸¹C. V. Tran and J. C. Bowman, “Robustness of the inverse cascade in two-dimensional turbulence,” *Phys. Rev. E* **69**, 036303 (2004).
- ⁸²M. Chertkov, C. Connaughton, I. Kolokolov, and V. Lebedev, “Dynamics of energy condensation in two-dimensional turbulence,” *Phys. Rev. Lett.* **99**, 084501 (2007).
- ⁸³P. Fischer and C.-H. Bruneau, “Wavelet-based analysis of enstrophy transfers in two-dimensional turbulence,” *Phys. Fluids* **21**, 065109 (2009).
- ⁸⁴K. Ohkitani, “Wave number space dynamics of enstrophy cascade in a forced two-dimensional turbulence,”

- Phys. Fluids A **3**, 1598 (1991).
- ⁸⁵A. Babiano and Antonello P., "Coherent vortices and tracer cascades in two-dimensional turbulence," J. Fluid Mech. **574**, 429–448 (2007).